GLOBAL IMAGE MATCHING BASED ON FEATURE POINT CONSTRAINED MARKOV RANDOM FIELD MODEL FOR PLANETARY MAPPING

Man Peng[1], Yiliang Liu[2], Zhaoqin Liu[3] and Kaichang Di[*4]
[1]Graduate Student, Institute of Remote Sensing Applications, Chinese Academy of Sciences
P. O. Box 9718, Datun Road, Chaoyang District, Beijing 100101, China; Tel: +86-010-64807987
Email: pengman@irsa.ac.cn

[2]Graduate Student, Institute of Remote Sensing Applications, Chinese Academy of Sciences
P. O. Box 9718, Datun Road, Chaoyang District, Beijing 100101, China; Tel: +86-010-64807987
Email: ylliu@irsa.ac.cn

[3]Associate Professor, Institute of Remote Sensing Applications, Chinese Academy of Sciences
P. O. Box 9718, Datun Road, Chaoyang District, Beijing 100101, China; Tel: +86-010-64807987
Email: liuzq@irsa.ac.cn

[4]Professor, Institute of Remote Sensing Applications, Chinese Academy of Sciences
P. O. Box 9718, Datun Road, Chaoyang District, Beijing 100101, China; Tel: +86-010-64868229
E-mail: kcdi@irsa.ac.cn

KEY WORDS: planetary mapping, global image matching, Markov Random Field, orbital imagery, rover imagery

ABSTRACT: In planetary exploration missions, high accuracy mapping from orbital and rover images is fundamentally important for scientific investigation, landing-site selection, precision landing, and rover navigation. Stereo image matching is a critical technique for 3D planetary mapping. A new global image matching method is presented based on feature points and Markov Random Field (MRF) model. The method extracts feature points, predicts disparity range, minimizes energy function of MRF, and consequently gets dense matching results. Experimental results using rover images from the Mars Exploration Rover mission and orbital images from Chang'E-1 lunar mission are presented to demonstrate the effectiveness of the proposed method.

1. INTRODUCTION

Planetary exploration usually includes orbital and rover missions. Orbital images map the planet globally and provide geometrical and spectral information for landing-site selection and precision landing; rover images provide more detailed information of the landing site for daily mission operations on the planet's surface. In recent years many studies have been conducted on geometric modeling and stereo mapping from orbital images (Albertz et al., 2005; Kirk et al., 2008; Li et al., 2011) and rover images (Deen and Lorre, 2005; Li et al., 2005). Stereo image matching is of great importance for 3D terrain construction in planetary mapping using orbital or rover images. Comparing with earth remote sensing images, orbital images of planetary surfaces (e.g., Moon and Mars surfaces) are usually lack of texture. For rover images of planetary surfaces, in addition to low texture, range discontinuities usually exist along the boundaries of prominent features such as large ridges and rocks. These pose special challenges to image matching and 3D terrain reconstruction.

A large number of stereo matching methods have been developed (Scharstein and Szeliski, 2002). Among various image matching methods, global image matching methods generally perform better than local image matching method in dealing with low-texture areas, parallax discontinuities and occlusions. So far, many global matching methods, e.g., Markov Random Field (MRF) based method, have been proposed for 3D modeling in computer vision applications (Szeliski et al., 2006). However, little research on global image matching has been conducted in planetary mapping. It is desirable to study global image matching method for precision planetary mapping purpose.

This paper presents a new method of matching based on feature point constrained MRF model for Mars and Lunar images. The rest of the paper is organized as follows: Section 2 describes the proposed method; Section 3 shows the experimental results using orbital and rover images respectively; Conclusions are given in Section 4.

2. FEATURE POINT CONSTRAINED MARKOV RANDOM FIELD METHOD

The new global image matching method is based on integration feature point matching and MRF model, which we call it Feature Point constrained Markov Random Field method (FP-MRF). The main idea is to use reliable feature

*Corresponding author

matching result to guide and control the global optimization of MRF so that to improve the efficiency and accuracy of the global matching. Figure 1 shows the processing flowchart of the method. Firstly feature points are extracted and matched from stereo images; and then feature points are used to predict disparities (parallaxes) of the remaining pixels. Next, image matching is applied using normalized correlation coefficient to get initial disparities. The initial dense matching result is refined through global optimization of an energy function of MRF. The global image matching runs iteratively over the full overlapped area until disparity labeling is stabilized. Finally the global matching result is refined with least squares matching to reach sub-pixel accuracy. Technical details of the method are given in the flowing subsections.

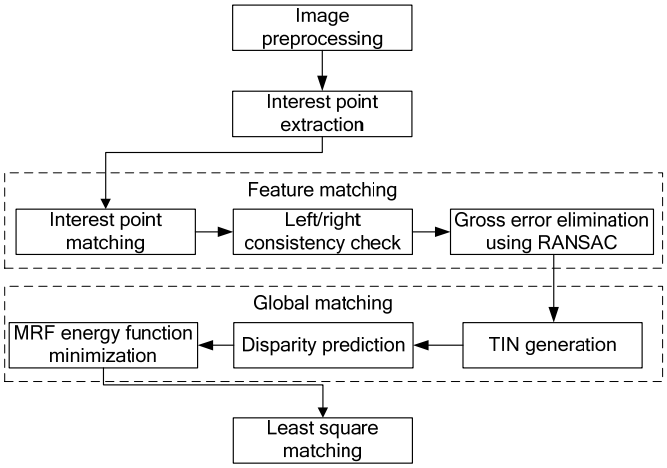

Figure 1. Flowchart of FP-MRF global image matching.

3.1 Feature point extraction and matching

After image preprocessing using Gaussian filter and histogram normalization to remove noises and illumination differences, feature points are extracted by Förstner operator according to Equation (1).

$$F(g) = \frac{g_x^2 g_y^2 - g_{xy}^2}{g_x^2 + g_y^2} \tag{1}$$

where $F(g)$ is the feature value of an image point; g_x, g_y are 1D gradients of point; g_{xy} is a 2D gradient. To extract sufficient feature points, the image point with the local maximum feature value in a 3*3 grid is considered as a feature point. Feature point matching is performed using normalized cross correlation coefficient. Matching error detection is firstly performed using left/right consistency check. Further matching error detection is conducted using a RANSAC (Fischler and Bolles, 1981) algorithm with similarity transformation model in a local area. After matching error elimination, the remaining matched feature points are used for subsequent global matching.

3.2 Global image matching

3.2.1 FP-MRF model: In this model, stereo matching is considered as a pixel labeling problem, which is naturally represented in terms of energy minimization. The energy function has two terms: one term penalizes solutions that are inconsistent with the observed data, while the other term enforces some kind of spatial coherence. Stereo matching is formulated to find a disparity function d that minimizes the following energy function.

$$E_{energy}(d) = E_{data}(d) + \beta E_{smooth}(d) \tag{2}$$

where the data term $E_{data}(d)$ measures how well the disparity fits the given stereo image pair, the smoothness term $E_{smooth}(d)$ encodes a smoothness assumption on disparity, and β is a weight to balance these two terms.

The data term is always measured by the difference between pixels and corresponding homologous points. Using a fixed window centered at the current pixel, correlation coefficient performs poorly in the vicinity of intensity edges and poorly textured regions. To overcome this problem, we use multi-window correlation in FP-MRF to measure their dissimilarity. For each pixel, image correlation is performed using nine different windows in which the current pixel is in different locations in the windows; the disparity with the maximum correlation coefficient ρ is taken as the output of the multi-window correlation. The value of ρ ranges from -1 to 1. To avoid inverse correlations we define the data term as

$$E_{data}(d) = \sum_{(x,y)} (2 - \rho(x,y) \times \rho(x,y)) \tag{3}$$

The smoothness term encodes the smoothness assumptions to make the optimization computationally tractable. The smoothness is restricted to only measuring the differences between neighboring pixel's disparities. The common used function is the truncated linear model, where the cost increased linearly based on the distance between the labels $f(p)$ and $f(q)$,

$$f(p,q) = \min(\tau, |f(p) - f(q)|) \tag{4}$$

where $f(p,q)$ is disparity discontinuity cost, τ controls when the cost stops increasing. So the smoothness term is

$$E_{smooth}(d) = \sum_{p,q \in N} f(p,q) \tag{5}$$

3.2.2 Disparity range prediction: Many existing global matching algorithms set the same disparity range for all the pixels. This makes the disparity space very large and energy minimization very slow. Since feature points have been reliably matched, we can get disparity range for each pixel adaptively. We use both grid and triangulated irregular network (TIN) to assign disparity range to each pixel. For an unmatched point in left image, its disparity range is computed through linear interpolation of parallaxes from vertices of the triangle that covers the point. Meanwhile, the image is divided in to several grids and the disparity range for an unmatched point is also predicted from neighborhood grids. Disparity range from grids is utilized to better handle discontinuities in places where linearity assumption might be violated.

As shown in Figure 2, black square represents unmatched point P; small black triangles are matched feature points; blue squares are 3×3 neighborhood grids, which are numbered as 0,1,2…8; red square is the grid where P located. The prediction steps are as follows:

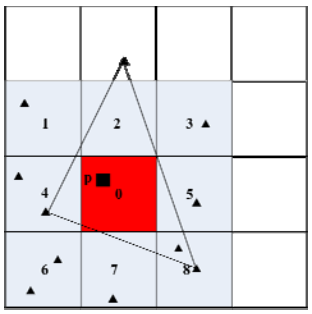

Figure 2. Disparity range estimation.

(1) Search the triangle where P located, the disparity of P is calculated by linear interpolation:

$$d_P = ax_P + by_P + c \tag{7}$$

where d_P is the interpolated disparity of P, x_P, y_P are coordinates of P, a,b,c are coefficients determined by coordinates and disparities of the three vertexes. Then the disparity range at P is set as

$$D1 = \{d \mid d_P - r \le d \le d_P + r\} \tag{8}$$

where $D1$ is disparity range set after linear interpolation, r is the searching step-size.

(2) Search the red grid index where P located, which is 0 in Figure 2, and get disparity set of all feature point in its 3×3 neighborhood grid, new disparity D2 is

$$D2 = \{\{d_1 - r, d_1, d_1 + r\} \cup \{d_2 - r, d_2, d_2 + r\} \cdots \cup \{d_n - r, d_n, d_n + r\}\} \tag{9}$$

where n is the number of all feature points in the 3×3 neighborhood, $n = 10$ in Figure 2.

(3) Compute the union of two sets $D1$ and $D2$, and set it as the final disparity range of P.

3.2.3 Minimization of energy function: The belief propagation (BP) algorithm works by passing messages around the graph defined by the four-connected image grid. A message presents the probability that the receiver should be at a disparity according to all information from the sender up to the current iteration. BP's message passing provides a time-varying adaptive support region for stereo matching to deal with textureless regions and depth discontinuities (Sun et al, 2003). In order to improve the efficiency of global matching, we use hierarchical belief

propagation (HBP) (Felzenszwalb et al, 2006) to estimate the minimum of energy function. HBP uses negative log probabilities to transfer max-product to min-sum, and consider linear time message updates, bipartite graph message passing schedule and multi-grid techniques to speed up the algorithm. Let $m^t_{p\to q}$ be the message that node p sends to its neighboring node q at iteration t, all entries in four directions are initialized to zero, and then new messages are computed iteratively as

$$m^t_{p\to q}(f_q) = \min_{f_p}\left(f(p,q) + E_{data}(f_p) + \sum_{s\in N(p)\setminus q} m^{t-1}_{s\to p}(f_p) \right) \tag{10}$$

where $N(p)\setminus q$ represents neighbors of p other than q. After iterations, a belief vector is computed for each node:

$$b_q(f_q) = D_q(f_q) + \sum_{p\in N(q)} m^T_{p\to q}(f_q) \tag{11}$$

Finally, the label f^*_q that minimizes $b_q(f_q)$ individually at each node is selected as the final matching result.

4. EXPERIMENTAL RESULTS

4.1 Pancam images of Mars Exploration Rover (MER)

Pancam is a pair of stereo cameras mounted on the camera bar of the rover with the stereo base line of 30 cm and the field of view of 16.8°×16.8°. The stereo images have been used to generate a series of mapping products to support mission operations (Di et al., 2008). The mapping capability of Pancam (the measurement error) is less than 1m within a range of 55m (Di et al., 2007). In this research, we use the epipolar-resampled stereo images (FFL files) to test our new matching method. The associated range maps (RNL files) are also downloaded for comparison purpose. Both image and range data can be downloaded from the website of MER Analyst's Notebook (http://an.rsl.wustl.edu/mer/mera/mera.htm), which is a node of NASA's Planetary Data System (PDS).

We have tested the proposed method using Pancam data acquired by Spirit rover at positions AACI (sol 488). A stereo pair are shown in Figure 3(a) and (b) respectively. After feature point matching and outlier elimination, 3500 points are matched. TIN and feature points are shown in Figure 4(a). Figure 4(b) and (c) show range map from PDS and our method respectively. In the two range maps, black areas represent pixels with no homologous points. It can be observed that the new method significantly reduced discontinuity areas. Moreover, DEM and DOM are generated and are shown in Figure 5. Fine details of the terrain are revealed in the DEM, showing that the developed global image method is effective.

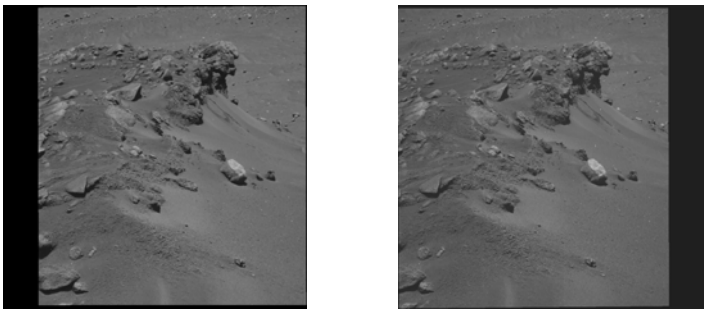

(a) (b)

Figure 3. Pancam stereo images acquired by Spirit rover.

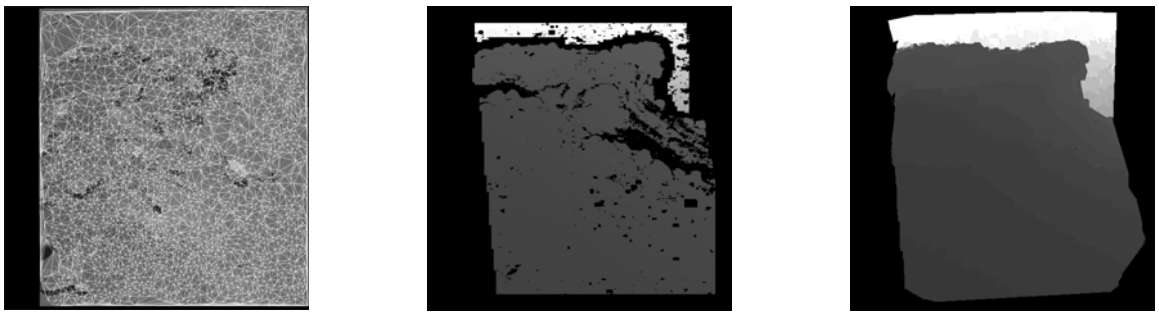

(a) Matched feature points and TIN (b) Range map from PDS (c) Range map from our method

Figure 4. Feature points, TIN and range maps.

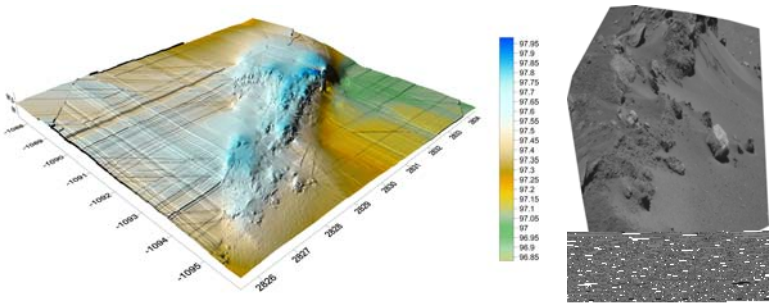

(a)DEM (b) DOM

Figure 5. DEM and DOM.

4.2 CE-1 CCD stereo images

China's first lunar probe Chang'E-1 (CE-1) carried a three line pushbroom CCD camera to map the moon surface in 3D. At a 200 km altitude, the image spatial resolution is 120 m and the swath width is about 60 km (Li et al, 2010). CE-1 CCD images have been released for public access. To test effectiveness of the proposed method for poor texture image, CE-1 stereo images (Level 1 product) of a 61km by 120 km area are used in the experiment. The image is 512 columns by 1001 rows, centered at 64S and 25E. The forward- and backward-looking images are shown in Figure 6(a) and (b) respectively. Overall, the textures are poor and challenging stereo matching.

After feature point matching and error elimination, 2468 points are matched and are used to control the consequent global dense matching. Disparity map after FP-MRF global matching are shown in Figure 6 (c). In order to show the terrain map more directly, 3D coordinates in LBF are transformed into longitude, latitude and altitude. Figure 7 (a) is a perspective view of the generated DEM, and (b) is the generated DOM overlaid on the DEM. It can be seen the terrain details particularly the craters are revealed in the DEM.

(a) Left image (b) Right image (d) Disparity map

Figure 6. CE-1 images and matching result.

(a)DEM (b) DOM

Figure 7. CE-1 DEM and DOM.

5. CONCLUSIONS

In this research we proposed a global image matching method named as FP-MRF for planetary mapping. The method is flexible in terms of incorporating feature point and constraints. Experimental results using Spirit rover data and

CE-1 CCD images demonstrated the effectiveness and high accuracy of the new method in dealing with regions of poor texture and/or range discontinuities. Further research will be performed to improve the computational efficiency of the global image matching method. And more planetary data will be used for validation of the new method.

Acknowledgements: Funding of this research by National Natural Science Foundation of China (40871202, 41002120) is acknowledged.

References

Albertz, J., M. Attwenger, J. Barrett, S. Casley, P. Dorninger, E. Dorrer, H. Ebner, S. Gehrke, B. Giese, K. Gwinner, C. Heipke, E. Howington-Kraus, R. L. Kirk, H. Lehmann, H. Mayer, J. Muller, J. Oberst, A. Ostrovskiy, J. Renter, S. Reznik, R. Schmidt, F. Scholten, M. Spiegel, U. Stilla, M. Wählisch, and G. Neukum, 2005. HRSC on Mars express - Photogrammetric and cartographic research. Photogramm. Eng. Remote Sens., 71(10), pp. 1153-1166.

Deen, R. G., and J. J. Lorre, 2005. Seeing in Three Dimensions: Correlation and Triangulation of Mars Exploration Rover Stereo Imagery. In Proceedings of the 2005 IEEE Conference on Systems, Man, and Cybernetics.

Di, K., and R. Li, 2007. Topographic mapping capability analysis of Mars exploration rover 2003 mission imagery, Proceedings of the 5th International Symposium on Mobile Mapping Technology (MMT 2007), 28-31 May, Padua, Italy, unpaginated CD-ROM.

Di, K., F. Xu, J. Wang , S. Agarwal, E. Brodyagina, R. Li, L. Matthies, 2008. Photogrammetric processing of rover imagery of the 2003 Mars Exploration Rover mission. ISPRS Journal of Photogrammetry and Remote Sensing ,63(2), pp. 181-201.

Felzenszwalb, P., and D. Huttenlocher, 2006. Efficient belief propagation for early vision. International Journal of Computer Vision, 70(1), pp. 41-54.

Fischler, M.A., and R.C. Bolles, 1981. Random sample consensus: a paradigm for model fitting with applications to image analysis and automated cartography. Graphics and Image Processing, 24(6), pp. 381-395.

Kirk, R. L., E. Howington-Kraus, M. R. Rosiek, J. A. Anderson, B. A. Archinal, K. J. Becker, D. A. Cook, D. M. Galuszka, P. E. Geissler, T. M. Hare, I. M. Holmberg, L. P. Keszthelyi, B. L. Redding,W. A. Delamere, D. Gallagher, J. D. Chapel, E. M. Eliason, R. King, and A. S. McEwen, 2008. Ultrahigh resolution topographic mapping of Mars with MRO HiRISE stereo images: Meter-scale slopes of candidate Phoenix landing sites. J. Geophys. Res., 113, pp. E00A24.

Li, C., J. Liu, X. Ren, L. Mou, Y. Zou, H. Zhang, C. L, J. Liu, W. Zuo, Y. Su, W. Wen, W. Wen, B. Zhao, J. Yang, X. Zou, M. Wang, C. Xu, D. Kong, X. Wang, F. Wang, L. Geng, Z. Zhang, L. Zheng, X. Zhu, J. Li, 2010. The Global Image of the Moon by the Chang'E-1: Data Processing and Lunar Cartography. Sci China Earth Sci, 53(8), pp. 1091-1102.

Li, R., S. W. Squyres, R. E. Arvidson, B. A. Archinal, J. Bell, Y. Cheng, L. Crumpler, D. J. Des Marais, K. Di, T. A. Ely, M. Golombek, E. Graat, J. Grant, J. Guinn, A. Johnson, R. Greeley, R. L. Kirk, M. Maimone, L. H. Matthies, M. Malin, T. Parker, M. Sims, L. A. Soderblom, S. Thompson, J. Wang, P. Whelley, and F. Xu, 2005. Initial results of rover localization and topographic mapping for the 2003 Mars exploration rover mission. Photogramm. Eng. Remote Sens., 71(10), pp. 1129-1142.

Li, R., J. Hwangbo, Y. Chen, K. Di, 2011. Rigorous Photogrammetric Processing of HiRISE Stereo Imagery for Mars Topographic Mapping. IEEE Transactions on Geoscience And Remote Sensing, 49(7), pp. 2558-2572.

Scharstein, D., and R. Szeliski, 2002. A taxonomy and evaluation of dense two-frame stereo correspondence algorithms. International Journal of Computer Vision, 47(1), pp. 7-42.

Szeliski, R., R. Zabih, D. Scharstein, O. Veksler, V. Kolmogorov, A. Agarwala, M. Tappen, and C. Rother, 2006. A comparative study of energy minimization methods for markov random fields. Computer Vision ECCV 2006, pp. 16-29.

Sun, J., N. Zheng, and H. Shum, 2003. Stereo matching using belief propagation. IEEE transactions on pattern analysis and machine intelligence, 25(7), pp. 787-800.